Defect-like Structures of Graphene on Copper Foils for Strain Relief Investigated by High-Resolution Scanning Tunneling Microscopy

Yanfeng Zhang,[†,‡,§] Teng Gao,[†,§] Yabo Gao,[†,§] Shubao Xie,[†] Qingqing Ji,[†] Kai Yan,[†] Hailin Peng,[†] and Zhongfan Liu[†,*]

[†]Center for Nanochemistry (CNC), Beijing National Laboratory for Molecular Sciences, State Key Laboratory for Structural Chemistry of Unstable and Stable Species, College of Chemistry and Molecular Engineering, Academy for Advanced Interdisciplinary Studies, Peking University, Beijing 100871, People's Republic of China and [‡]Deparment of Advanced Materials and Nanotechnology, College of Engineering, Peking University, Beijing 100871, People's Republic of China. [§] These authors contributed equally to this work.

ABSTRACT Understanding of the continuity and the microscopic structure of as-grown graphene on Cu foils through the chemical vapor deposition (CVD) method is of fundamental significance for optimizing the growth parameters toward high-quality graphene. Because of the corrugated nature of the Cu foil surface, few experimental efforts on this issue have been made so far. We present here a high-resolution scanning tunneling microscopy (STM) study of CVD graphene directly on Cu foils. Our work indicates that graphene can be grown with a perfect continuity extending over both crystalline and noncrystalline regions, highly suggestive of weak graphene—substrate interactions. Due to thermal expansion mismatch, defect-like wrinkles and ripples tend to evolve either along the boundaries of crystalline terraces or on noncrystalline areas for strain relief. Furthermore, the strain effect arising from the conforming of perfect two-dimensional graphene to the highly corrugated surface of Cu foils is found to induce local bonding configuration change of carbon from sp^2 to sp^3, evidenced by the formation of "three-for-six" lattices.

KEYWORDS: graphene · STM · CVD · Cu foil · growth

Graphene, a monolayer of sp^2-bonded carbon atoms packed into a two-dimensional honeycomb lattice, has attracted tremendous interest because of its unique linear energy band near the Fermi energy and concomitant novel physical and chemical properties.[1−7] Graphene has very high carrier mobility and perfect optical transparency (up to 90%), which makes it an ideal material for various applications such as transparent electrodes, transistors, and spintronic devices. For these applications, it is still challenging to produce large-area uniform graphene with low defects and controlled thicknesses. An affordable and practical chemical vapor deposition (CVD) method has been recently developed to prepare graphene on Cu foils through the decomposition of methane at high temperature. The limited solubility of carbon into Cu results in perfect monolayer graphene with dimensions even up to tens of inches.[8−15] The capability of transferring CVD graphene onto arbitrary substrates promotes its wide applications.

Investigations on the continuity and the microscopic feature of graphene prepared with various methods are very crucial for understanding their novel physical properties, such as the transport property. Scanning tunneling microscopy (STM) can be an ideal analytical method, by which the atomic-scale structures of exfoliated graphene transferred onto SiO_2 and epitaxial graphene made under high vacuum conditions have been reported in recent works.[16−22] With reference to graphene on Cu, only two typical results were presented using STM.[23,24] The low-pressure CVD growth was incorporated into the high-vacuum STM to prepare graphene on single-crystalline Cu(111) substrates.[23] Preferred orientations of graphene flakes are confirmed by high-resolution STM observations, which accounts for relative strong coupling of graphene with Cu(111). A more recent work focused on the structure of graphene on multiple facets of polycrystalline Cu, where both honeycomb lattices and Moiré patterns were obtained.[24] Obviously, the unpolished surface of Cu foils is very different from the above two cases, and the above graphene growth should be strongly influenced by the substrate effect. Up to now, no atomic-scale STM studies have been performed on the widely used CVD graphene on the Cu foil system.

In this work, we demonstrate systematic STM observations of as-grown CVD

* Address correspondence to zfliu@pku.edu.cn.

Received for review February 12, 2011 and accepted April 18, 2011.

Published online April 18, 2011
10.1021/nn200573v

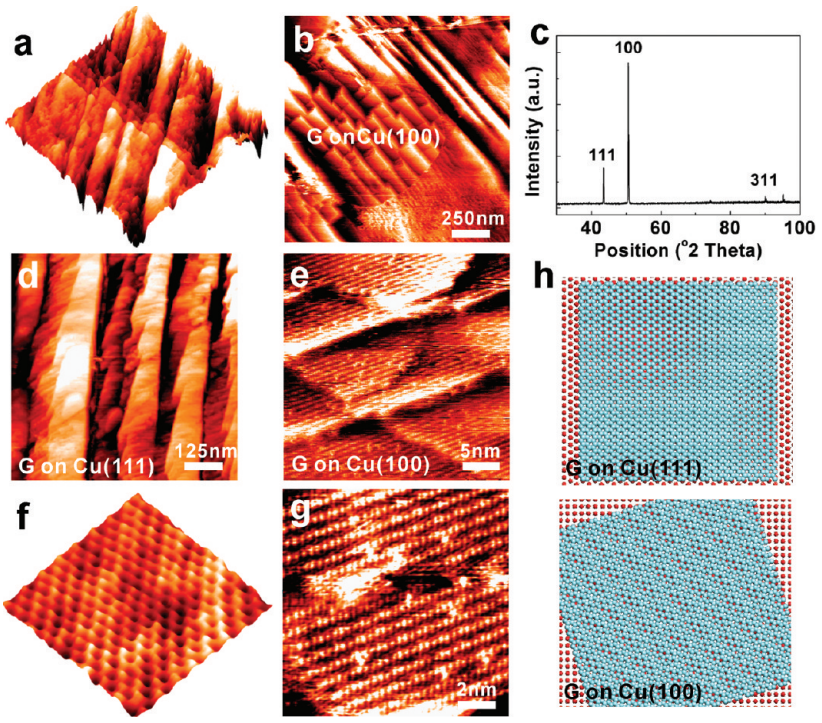

Figure 1. (a,b) Large-scale STM images of Cu foils after CVD growth (1500 nm × 1500 nm; $V_{Bias} = -0.45$ V, $I_T = 3.7$ nA). (c) Powder X-ray diffraction pattern of the sample surface. (d) Graphene growth on terraced Cu(111) (750 nm × 750 nm; $V_{Bias} = -0.002$ V, $I_T = 4.0$ nA) confirmed by the hexagonal carbon lattice in (f) (3.8 nm × 3.8 nm). (e,g) Formation of square-shaped Moiré patterns on terraced Cu(100): (e) 30 nm × 30 nm) and (g) 11.5 nm × 11.5 nm ($V_{Bias} = -0.05$ V, $I_T = 5.0$ nA). (h) Schematic diagram showing the formation of hexagonal carbon lattices and Moiré patterns on (111) and (100) facets of Cu, respectively.

graphene on Cu foils. The continuity of graphene over macroscopic scales was studied. It is found that graphene patches can span over several micrometers inside a single domain, and the domain orientation shows almost no relation with the substrate symmetry. The microscopic structures of monolayer graphene, such as hexagonal carbon lattices, wrinkles, and ripples, which cannot be fully recognized by other surface analysis methods, were achieved. The different thermal expansion behavior between graphene and Cu is considered to induce residual strains through thermal quenching, released by the formation of wrinkles or ripples. In addition, the strain effect originating from the conforming of the two-dimensional graphene to the corrugated surface of Cu foils is thought to result in local bonding change of carbon from sp^2 to sp^3. Small patches of "three-for-six" lattices evolve among normal hexagonal lattices. Moreover, the initial growth of bilayer graphene was also examined through atomically resolved STM observations. The AB stacking geometry of the bilayer region is identified.

RESULTS AND DISCUSSION

The growth of large-scale uniform monolayer graphene was completed by cracking methane over Cu foils at a high temperature of ~1000 °C followed by thermal quenching. As the growth temperature is very close to the melting point of Cu (~1083 °C), adsorption of carbon fragements and desorption of Cu atoms can bring about dramatic changes of the surface morphology. This has been verified by a recent *in situ* low-energy electron microscopy (LEEM) investigation at the growth state, where considerable Cu sublimation occurs, leading to corrugated Cu surfaces.[25] Note that the imaging scale of LEEM is usually limited to 1 μm, by which the microscopic structure of graphene cannot be revealed at the as-grown state.

Here, STM is utilized to show the surface morphology of graphene after CVD growth. Figure 1a (1500 nm × 1500 nm) presents some stripe-like structures with lateral dimensions of several hundred nanometers. Close-up views of the region usually show terraces and steps, as is comparable with that of single-crystal surfaces. Clear transitions from crystalline to noncrystalline states can be observed from similar large-scale STM images, as exemplified in Figure 1b (1500 nm × 1500 nm). In order to know the surface crystallization feature, powder X-ray diffraction patterns are recorded and displayed in Figure 1c, where the (111) and (100) facets can be found to orient in the vertical direction. These preferred facets should correspond to the crystalline regions presented in Figure 1a,b. Since the two low-index facets have a hexagonal or a cubic atomic arrangement, the above graphene growth should be strongly influenced by the different symmetries. A zoom-in image reveals the terraces of Cu but with limited sizes (Figure 1d). The height of the terrace is measured to be a multiple of ~0.26 nm by STM height

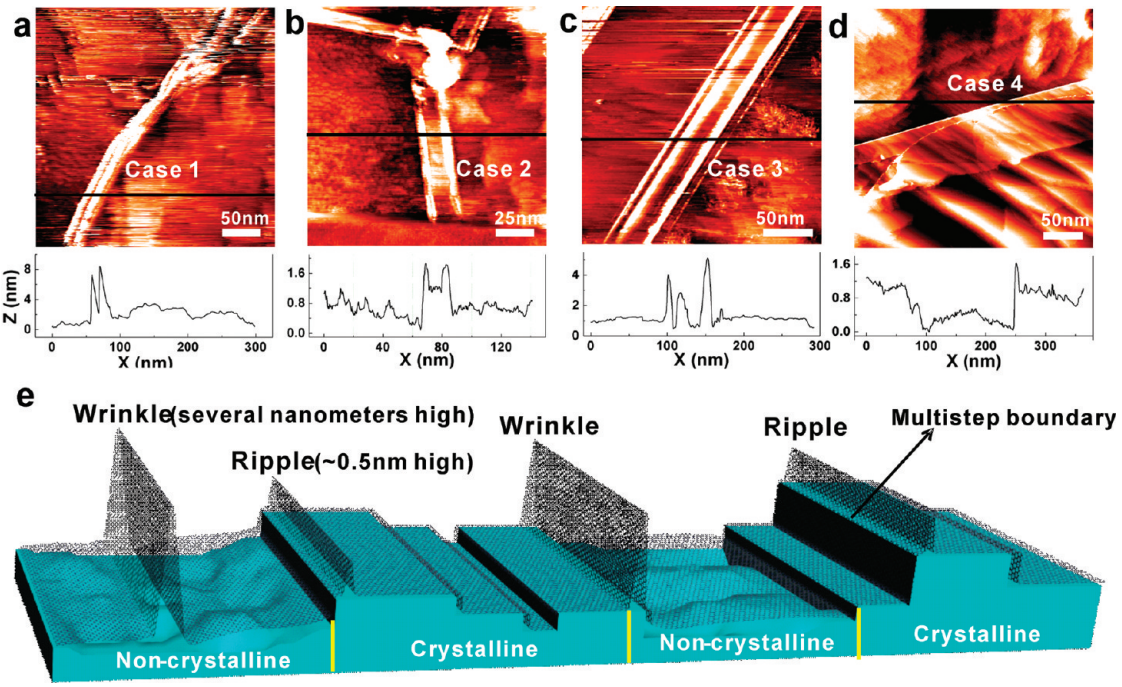

Figure 2. (a) STM morphology of crooked wrinkles (300 nm × 300 nm) on amorphous Cu substrates and its height profile along the line direction (case 1). (b,c) Striped ripples and wrinkles evolving along the boundaries from crystalline to noncrystalline states (cases 2 and case 3): (b) 150 nm × 150 nm and (c) 300 nm × 300 nm. (d) Ripples appearing on step boundaries of crystalline Cu (case 4) (370 nm × 370 nm). All of the STM images are captured with $V_{Bias} = -0.2$ V, $I_T = 2.0$ nA. (e) Sketch map showing the positions of wrinkles and ripples with substrate states.

profiles. In an atomic-scale STM image captured on the terrace (Figure 1f), a hexagonal lattice with a lattice constant of ~0.246 nm appears to show a perfect agreement with the known lattice constant of monolayer graphene. This is a result of the relative match of the lattice constants of graphene (0.246 nm) and Cu(111) facets (0.256 nm). It is worthy to note that relative rotations of the two lattices to form Moiré patterns are probable, while this is not seen in this work. Besides, the height profile along the horizontal line in Figure 1f presents a surface roughness of ~0.05 nm over a lateral distance of ~5 nm (not shown here).

A novel large-period superstructure having a nearly quadrilateral lattice (0.8 nm × 0.4 nm) can also be observed frequently on step bunching regions (Figure 1e,g), where the terrace size is limited to only several square nanometers. Interestingly, the appearance of this superstructure depends on the applied bias. A close tip−sample condition or a low bias usually results in a perfect imaging of the hexagonal lattice (not shown here). The origin of this periodic modulation on monolayer graphene can be attributed to the formation of so-called Moiré patterns caused by interference effects between upper carbon lattices and (100) facets of Cu, as was similarly reported for graphene growth on multiple facets of polycrystalline Cu.[24] As a summary, a schematic diagram is given in Figure 1h to illustrate the formation of hexagonal carbon lattices and rectangular Moiré patterns on Cu(111) and Cu(100), respectively.

Besides the observation of carbon lattices on terraced regions, other obvious surface features that can be easily imaged are some striped contrasts of several hundred nanometers long. Figure 2a demonstrates two linked striped contrasts on the noncrystalline surface, which manifests an average height of ~6 nm and a width of 10−20 nm. The striped contrasts have dimensions corresponding well with that of the wrinkled structures in graphene growth, thus called wrinkles in this work. At the transition regions from crystalline to amorphous states around the step boundaries, some line-shaped STM contrasts (~0.5 nm in height and ~10 nm in width) can also be obtained with their dimensions readable from the height profile measurement as listed below (Figure 2b). These line-shaped structures have a limited height (usually <1 nm, and mostly ~0.5 nm), which is in line with the so-called ripple as reported before.[16−18,26−28] It is interesting to see that wrinkles of several nanometers high can also evolve around the transition regions, as exemplified in Figure 2c. Moreover, the multistep boundary prefers to be occupied by wrinkles or ripples than other amorphous regions, and a ripple formation is presented in Figure 2d. On the basis of the above results, it can be summarized that graphene growth on the highly corrugated surface regions of Cu tends to be buckled up from the background, resulting in the formation of wrinkles or ripples (Figure 2b−d). A three-dimensional schematic map is provided in Figure 2e to correlate the substrate configurations with the positions of wrinkles

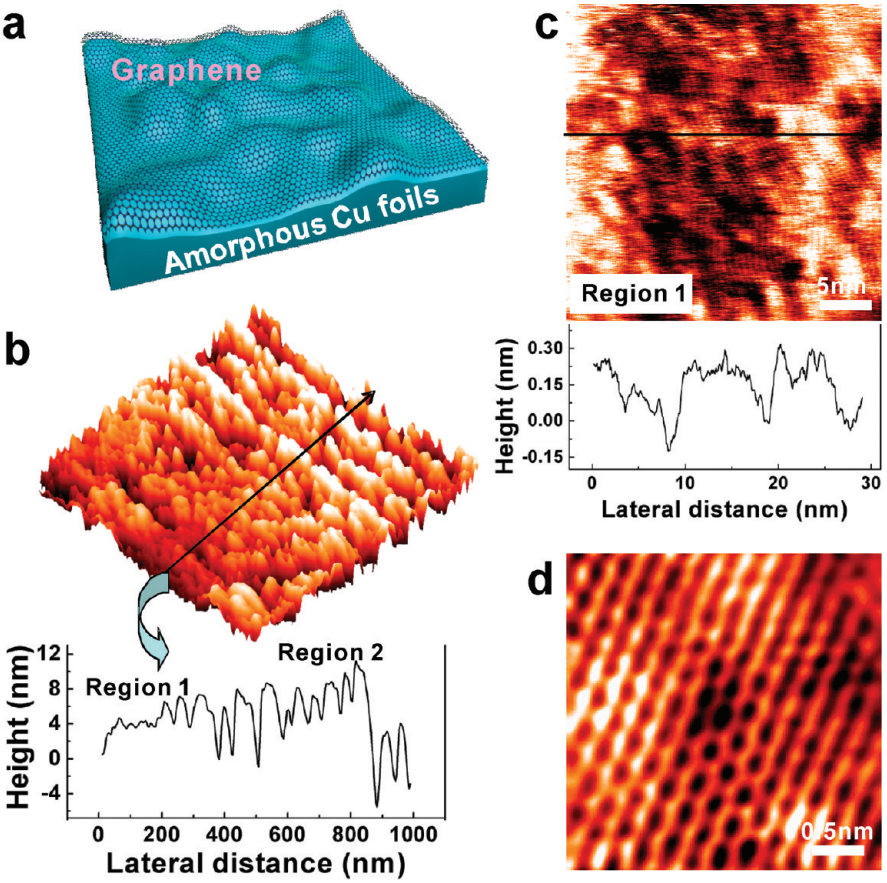

Figure 3. (a) Schematic drawing of graphene growth on amorphous surfaces of Cu foils. (b) Large-scale STM morphology (1000 nm × 1000 nm). (c) Zoom-in of relative flat regions (region 1) (29.2 nm × 29.2 nm). (b,c) Captured with $V_{Bias} = -0.002$ V, $I_T = 9.2$ nA. (d) Atomic-scale image (3.0 nm × 3.0 nm; $V_{Bias} = -0.002$ V, $I_T = 14.8$ nA) on the flat area of (c) with a hexagonal lattice.

and ripples. Statistically, the density of wrinkles and ripples is approximately $1/\mu m^2$.

The formation of wrinkles and ripples is believed to be closely related to the different in-plane thermal expansion behaviors between graphene and Cu. As reported before, the big difference in thermal expansion coefficients between metal substrates and graphite can result in more contraction of metals than that of graphite during thermal quenching, and the release of such compressive stress leads to the formation of wrinkles and ripples.[29] As is known, the thermal expansion coefficient of graphite changes from -1.25×10^{-6} to 1.25×10^{-6}/K in a temperature range from 293 to 1293 K. This indicates a nearly zero net uniaxial contraction of graphene during thermal quenching. The net uniaxial expansion ($\Delta L/L_{293}$) of Cu at 1200 K with respect to that at 293 K approaches 1.834%.[30] When the lateral dimension of a wrinkle is considered (~15 nm), the wrinkles having an average height of 6 nm need to be separated by ~1050 nm from each other. This is consistent with the experimental data ($1/\mu m^2$). This good coincidence may support our deduction that the driving force for the formation of wrinkles and ripples is the thermal expansion mismatch between graphene and Cu.

It is worth noting that these wrinkles can act as indicators for the formation of continuous graphene flakes since they can be easily identified from large-scale STM images. More importantly, as reported before, the local electronic structure or the local electric potential around the wrinkled regions can be substantially modulated.[20] It is meaningful to reduce the density of winkles and ripples so that the two-dimensional electronic property of graphene can be maintained.

Sufficient knowledge of the atomic-scale structure of graphene on rough Cu foils, as shown in the sketch map of Figure 3a, is highly necessary because the binding configuration of graphene may be altered by the rough surface of Cu foils. One of the typical STM morphologies with a scale of 1000 nm × 1000 nm is presented in Figure 3b. According to the line profile measurement, the surface roughness can be divided into two cases. It either attains ~1 nm in height over several tens of nanometers in the lateral distance or approaches several nanometers in height within the same lateral scale.

Magnified images on the lower left corner of Figure 3b (region 1) are captured in Figure 3c, in which

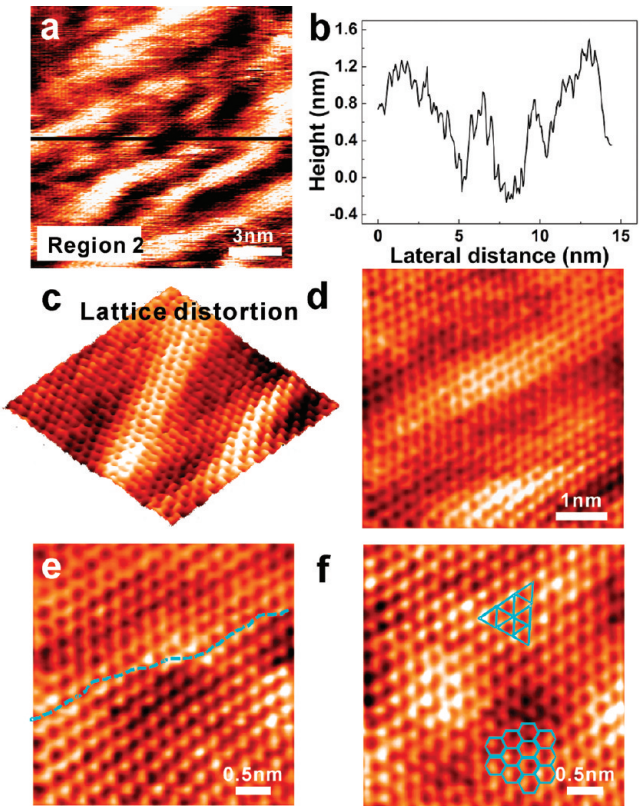

Figure 4. (a) Typical STM topography of graphene on highly corrugated surface regions (14.6 nm × 14.6 nm; $V_{Bias} = -0.002$ V, $I_T = 2.5$ nA). (b) Corresponding section view along the indicated line. (c,d) Three-dimensional and two-dimensional close-up images demonstrating clear lattice distortions (5.1 nm × 5.1 nm; $V_{Bias} = -0.002$ V, $I_T = 4.9$ nA). (e,f) Lattice configuration change from hexagons to triangles on the same regions as that of (a) (3.7 nm × 3.7 nm; $V_{Bias} = -0.002$ V, $I_T = 5.0$ nA). The two cases are separated by a dashed line in (e) and indicated by triangles and hexagons in (f).

the height profile plot illustrates a maximum height fluctuation of ~0.4 nm over a lateral distance of ~29.2 nm. In this relative flat region, it is probable to gain perfect hexagonal lattices with a lattice constant of ~0.246 nm, as exemplified in Figure 3d (3.0 nm × 3.0 nm). What merits our special attention is that the atomic structure can only be obtained under an ultimate condition of $V_{Bias} = -0.002$ V, $I_T = 14.8$ nA. Why is this extreme condition essential? In general, the observed hexagonal contrast by STM originates from both the electronic feature and the physical contour of the carbon lattice.[31] The substrate electronic structure can also imply strong effects on STM imaging. To avoid the substrate effect, a very close tip−sample distance is needed.

Further careful STM examinations indicate that not all of the CVD graphene presents perfect hexagonal lattices on rough surfaces of Cu foils. A typical STM result of the rough region (such as region 2 of Figure 3b) is displayed in Figure 4a, with an image scale of 14.6 nm × 14.6 nm. The height profile (Figure 4b) along the line in Figure 4a illustrates a surface roughness of ~1.5 nm over a lateral distance of ~14.6 nm. Evidently, this surface area is more corrugated than the one mentioned above (a maximum height fluctuation of ~0.4 nm over a lateral distance of ~29.2 nm). A sequential zoom-in STM image in a three-dimensional (3D) form is displayed in Figure 4c (5.1 nm × 5.1 nm), which provides a visual impression of the up-and-down surface. Its 2D image (Figure 4d) demonstrates a distinct lattice distortion from upper to lower parts. Except for lattice distortion, small graphene patches of hexagonal (upper left) and "three-for-six" lattices (lower right) appear alternatively, which are shown in Figure 4e,f (3.7 nm × 3.7 nm). In order to illustrate this, the two phases are divided by a dashed line in Figure 4e and differentiated by hexagonal and triangular grids in Figure 4f.

In published results, this lattice configuration transformation on graphene is explained by film curvature changes or charge traps.[16,20] The former case is reported only on ~3 nm high wrinkles for exfoliated graphene transferred onto SiO_2 substrates. The increased local curvature and the associated strain is regarded as the possible reason for breaking the six-fold symmetry and degenerating the electronic state of graphene, followed with the bonding feature alteration from sp^2 to sp^3. This mechanism should also be suitable for our graphene on Cu foil system. As mentioned above, graphene on a smooth Cu terrace only presents a total roughness of ~0.05 nm, a typical value for the apparent height of the carbon lattice, while in

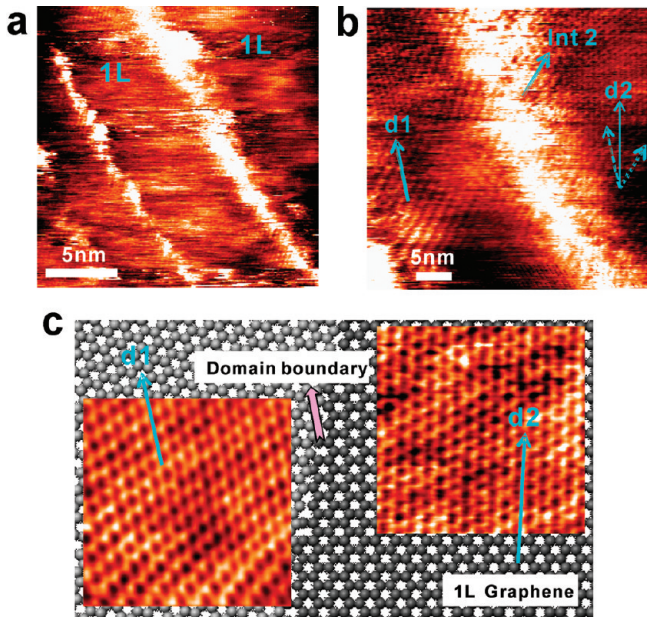

Figure 5. (a,b) Merging of monolayer graphene (1L) patches at line-shaped defects: (a) 20 nm × 20 nm and (b) 10 nm × 10 nm ($V_{Bias} = -0.002$ V, $I_T = 2.5$ nA). The orientations of the graphene patches are indicated with d1 and d2 in (b). The direction of the interference pattern (Int2) at the domain boundary is rotated by 30° with respect to d2. (c) Schematic diagram showing two graphene flakes with different orientations. The insets are the atomic-scale STM images on both sides of the defect line in (b).

Figure 4b, the corrugation of ~1.46 nm over a lateral distance of ~14.6 nm should be related to the undulation of the amorphous substrate. The conforming of 2D graphene to the highly corrugated substrate surface should lead to uneven strain effects and breaking of the six-fold symmetry of the carbon lattice. Three of the six atoms are lifted up to be out of the hexagonal ring, resulting in the unique "three-for-six" patterns in STM topographies. Note that this is the first demonstration where the corrugated surface associated strain can induce universally existing triangular carbon lattices. These regions with dimensions of several square nanometers interweave with the normal hexagonal lattices, leading to the formation of graphene domains over several micrometers. Graphene with "three-for-six" patterns deviates from the ideal two-dimensional state with slight three-dimensional components, evidenced by the bonding configuration change from sp^2 to sp^3. The local density of states (LDOS) for the "three-for-six" pattern is expected to be modified, as has been observed on the wrinkles of exfoliated graphene having "three-for-six" lattices with the appearance of midgap states by scanning tunneling spectroscopy (STS).[20,32−35] Here, due to the limitation of the STM apparatus, it is hard to get perfect STS spectra of the novel triangular lattice, but it is highly necessary and will be pursued in future works.

Understanding of the boundaries and the orientations of CVD graphene flakes is very crucial for further improving the uniformity of graphene and illustrating the limited carrier mobility of CVD graphene. Large-scale STM morphology (Figure 5a) is deliberately captured around two defect lines connecting three graphene patches. A close-up image on one of the defect lines demonstrates hexagonal lattices on both sides (Figure 5b). Their orientations (d1 and d2) can be judged by atomic-scale STM images, which are rotated by ~11° with respect to each other. The broken continuity at the defect line can also be identified by the occurrence of the $(\sqrt{3} \times \sqrt{3})R30°$ interference pattern (Figure 5b), having an orientation (Int2) rotated by 30° with d2.[36,37] To illustrate this, a schematic drawing is provided in Figure 5c, with atomic-scale images on both sides of the domain boundary inserted. Note that the electron scattering effect around the domain boundary can substantially reduce the carrier mobility of graphene. Decreasing the amount of domain boundary should be a key step for further enhancing the quality of CVD graphene. More systematic STM investigations indicate that the rotation angles between graphene flakes usually fall in the range of 11−30°, and no special orientation is more preferred than others, while the orientations of CVD graphene on single-crystal Cu(111) are usually strictly aligned or slightly misoriented with the substrate lattice.[23] As a result, an interaction of graphene with Cu foils that is weaker than that with Cu(111) can be inferred. That is why CVD graphene can be prepared with tenths of inches in size.

The CVD growth of graphene on Cu foils is widely considered to be dominated by a self-terminated process, where bilayers or trilayers contribute only a small portion of the surface (less than 5%). A recent effort confirmed the capability of achieving bilayer graphene of high homogeneity and wafer-scale size.[14] The bilayer nature was confirmed by Raman

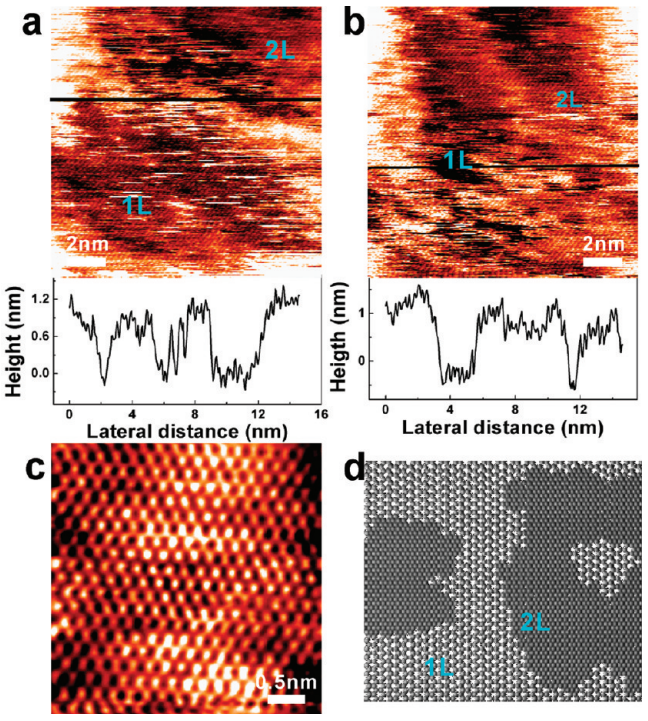

Figure 6. (a,b) STM morphologies of the initial growth of bilayer graphene (2L) and their height profiles along corresponding lines (14 nm × 14 nm; $V_{Bias} = -0.002$ V, $I_T = 2.5$ nA). (c) Atomic-scale resolution image of 2L areas with triangular lattices (3.7 nm × 3.7 nm; $V_{Bias} = -0.002$ V, $I_T = 12.5$ nA). (d) Sketch map of the stacking behavior of bilayer graphene patches.

spectroscopy, atomic force microscopy, and so on. Even so, other surface-sensitive analyses need to be supplied, such as atomically resolved STM, to explore its atomic structures and the stacking geometry. In this research, the morphology of the initial bilayer growth is shown in Figure 6a,b, which is mainly composed of high and low STM contrasts with unclear boundaries. Section-view measurements along the indicated lines give an average height difference of ~1.0 nm between the two typical contrasts. This value is much larger than a conventional interlayer distance of graphite or bilayer graphene (~0.34 nm). If the brighter regions are ascribed to the bilayers, the much wider interlayer distance is believed to originate from either the corrugated feature of the substrate or the electronic effect under the extreme scanning conditions.

In addition to height profile analysis, the existence of bilayers can be reconfirmed by high-resolution STM images. The atomic-scale STM images of the low-contrast regions usually reveal hexagonal lattices (not shown here), while on the brighter regions, triangular lattices typical for AB-stacked bilayer graphene can be noticed, as exemplified in Figure 6c. The meandering of molecule rows and the above uneven contrasts can be attributed to the influence of the corrugated surface of Cu foils. Moreover, on the basis of large-scale STM morphologies and height profile analysis, the bilayer regions can be estimated to be ~50 or ~90% of the scan areas (Figure 6a,b), respectively. A more quantitative evaluation of the bilayer area can be realized either by capturing more STM images and making statistics or by transferring graphene to other arbitrary substrates (like SiO_2) and using other methods such as Raman spectroscopy and optical microscopy.

Due to the low solubility of carbon into Cu, the growth of monolayer graphene mainly involves surface diffusion and nucleation processes. Once graphene flakes are formed, they expand their sizes and connect with other ones. This applies to the bilayer growth, hereby decreasing the nucleation site and increasing the surface mobility of carbon fragments should lead to larger domain sizes. The different thing is that the second carbon layer interacts with monolayer graphene by $\pi-\pi$ interactions, which is a little bit stronger than that of monolayer graphene with Cu foils. Consequently, the diffusion of graphene fragments should be limited, as evidenced by the appearance of very small graphene flakes and the randomly distributed pits at the initial growth stage (Figure 6a,b). In order to increase the continuity or the domain size of bilayers, some parameters, such as growth temperature, vacuum, cooling rate, and growth rate, need to be optimized. In a recent publication, increasing the activity of Cu catalysts was proven to be another candidate.[24]

CONCLUSION

High-resolution STM observations have been accomplished on as-grown CVD graphene on Cu foils. We find that graphene is weakly coupled with the

underlying Cu substrate, evidenced by its extra capability to span over crystalline and amorphous substrate regions. In order to release strain effects from the different thermal expansion behaviors between graphene and Cu, CVD graphene tends to be buckled up with the formation of wrinkles and ripples on highly corrugated surface regions. We also detect that interesting three-for-six lattices tend to form on high curvature surfaces to show another scope for releasing strain effects. In addition, we demonstrate atomically resolved STM investigations of the bilayer area and confirm its AB-stacking geometry.

Since the carrier mobility of graphene, a good parameter for judging its quality, can be strongly reduced by defects such as domain boundaries, point defects, and so on, adequate knowledge of the microscopic features of as-grown graphene is crucial for future experimental explorations about the novel physical and chemical properties, as well as reliable device applications.

EXPERIMENTAL SECTION

The graphene samples used in this work were prepared with ~25 μm thick Cu foils as substrates. The CVD growth method was described elsewhere.[8] The nominal monolayer graphene is actually composed of both monolayer patches (~90%) extending up to several micrometers in dimension and a few bilayer or trilayer patches (~10%) of very small domain sizes. This was confirmed by Raman spectroscopy measurements after chemical transferring graphene onto SiO_2 substrates. The bilayer sample was prepared by an epitaxial method with monolayer graphene as substrates.[38]

The atomic-scale characterization was realized using an ultrahigh vacuum (UHV) variable-temperature STM, equipped with molecular beam epitaxy (MBE) and low-energy electron diffraction (LEED) facilities. In order to achieve more stable STM images, annealing of the air-transferred sample was performed to remove the physisorbed organics and water. All of the STM images were captured with STM working at room temperature.

Acknowledgment. This work was financially supported by the National Natural Science Foundation of China (Grant Nos. 20973013, 51072004, 50821061, 20833001, 21073003) and The Ministry of Science and Technology of China (Grant Nos. 2007CB936203, 2007CB936802, 2011CB921903).

Note Added after ASAP Publication. After this paper was published ASAP April 25, 2011, a correction was made to reference 15. The revised version was published April 29, 2011.

REFERENCES AND NOTES

1. Geim, A. K.; Novoselov, K. S. The Rise of Graphene. *Nat. Mater.* **2007**, *6*, 183–191.
2. Castro Neto, A. H.; Guinea, F.; Peres, N. M.; Novoselov, K. S.; Geim, A. K. The Electronic Properties of Graphene. *Rev. Mod. Phys.* **2009**, *81*, 109–162.
3. Novoselov, K. S.; Geim, A. K.; Morozov, S. V.; Jiang, D.; Zhang, Y.; Dubonos, S. V.; Grigorieva, I. V.; Firsov, A. A. Electric Field Effect in Atomically Thin Carbon Films. *Science* **2004**, *306*, 666–669.
4. Novoselov, K. S.; Geim, A. K.; Morozov, S. V.; Jiang, D.; Katsnelson, M. I.; Grigorieva, I. V.; Dubonos, S. V.; Firsov, A. A. Two-Dimensional Gas of Massless Dirac Fermions in Graphene. *Nature* **2005**, *438*, 197–200.
5. Zhang, Y. B.; Tan, Y. W.; Stormer, H. L.; Kim, P. Experimental Observation of the Quantum Hall Effect and Berry's Phase in Graphene. *Nature* **2005**, *438*, 201–204.
6. De Heer, W. A.; Berger, C.; Wu, X.; First, P. N.; Conrad, E. H.; Li, X.; Li, T.; Sprinkle, M.; Hass, J.; Sadowski, M. L.; *et al.* Epitaxial Graphene. *Solid State Commun.* **2007**, *143*, 92–100.
7. Emtsev, K. V.; Bostwick, A.; Horn, K.; Jobst, J.; Kellogg, G. L.; Ley, L.; McChesney, J. L.; Ohta, T.; Reshanov, S. A.; Röhr, J.; *et al.* Towards Wafer-Size Graphene Layers by Atmospheric Pressure Graphitization of Silicon Carbide. *Nat. Mater.* **2009**, *8*, 203–207.
8. Li, X. S.; Cai, W. W.; An, J. H.; Kim, S.; Nah, J.; Yang, D. X.; Piner, R. D.; Velamakanni, A.; Jung, I.; Tutuc, E.; *et al.* Large-Area Synthesis of High-Quality and Uniform Graphene Films on Copper Foils. *Science* **2009**, *324*, 1312–1314.
9. Li, X. S.; Cai, W. W.; Colombo, L.; Ruoff, R. S. Evolution of Graphene Growth on Cu and Ni Studied by Carbon Isotope Labeling. *Nano Lett.* **2009**, *9*, 4258–4263.
10. Li, X. S.; Zhu, Y.; Cai, W. W.; Borysiak, M.; Han, B.; Chen, D.; Piner, R. D.; Colombo, L.; Ruoff, R. S. Transfer of Large-Area Graphene Films for High-Performance Transparent Conductive Electrodes. *Nano Lett.* **2009**, *9*, 4359–4363.
11. Levendorf, M. P.; Ruiz-Vargas, C. S.; Garg, S.; Park, J. Transfer-Free Batch Fabrication of Single Layer Graphene Transistors. *Nano Lett.* **2009**, *9*, 4479–4483.
12. Lee, Y.; Bae, S.; Jang, H.; Jang, S.; Zhu, S. E.; Sim, S. H.; Song, Y. I.; Hong, B. H.; An, J. H. Wafer-Scale Synthesis and Transfer of Graphene Films. *Nano Lett.* **2010**, *10*, 490–493.
13. Bae, S.; Kim, H.; Lee, Y.; Xu, X.; Park, J. S.; Zheng, Y.; Balakrishnan, J.; Lei, T.; Kim, H. R.; Song, Y. I.; *et al.* Roll-to-Roll Production of 30-Inch Graphene Film for ITO Replacement. *Nat. Nanotechnol.* **2010**, *5*, 574–578.
14. Lee, S.; Lee, K.; Zhong, Z. Wafer Scale Homogeneous Bilayer Graphene Films by Chemical Vapor Deposition. *Nano Lett.* **2010**, *10*, 4702–4707.
15. Li, X. S.; Magnuson, C. W.; Venugopal, A.; An, J. H.; Suk, J. W.; Han, B.; Borysiak, M.; Cai, W. W.; Velamakanni, A.; Zhu, Y.; Fu, L. F.; Vogel, E. M.; Voelkl, E.; Colombo, L.; Ruoff, R. S. Graphene Films with Large Domain Size by a Two-Step Chemical Vapor Deposition Process. *Nano Lett.* **2010**, *10*, 4328–4334.
16. Ishigami, M.; Chen, J. H.; Cullen, W. G.; Fuhrer, M. S.; Williams, E. D. Atomic Structure of Graphene on SiO_2. *Nano Lett.* **2007**, *7*, 1643–1648.
17. Stolyarova, E.; Rim, K. T.; Ryu, S. M.; Maultzsch, J.; Kim, P.; Brus, L. E.; Heinz, T. F.; Hybertsen, M. S.; Flynn, G. W. High-Resolution Scanning Tunneling Microscopy Imaging of Mesoscopic Graphene Sheets on an Insulating Surface. *Proc. Natl. Acad. Sci. U.S.A.* **2007**, *104*, 9209–9212.
18. Geringer, V.; Liebmann, M.; Echtermeyer, T.; Runte, S.; Schmidt, M.; Ruckamp, R.; Lemme, M. C.; Morgenstern, M. Intrinsic and Extrinsic Corrugation of Monolayer Graphene Deposited on SiO_2. *Phys. Rev. Lett.* **2009**, *102*, 076102(1−4).
19. Teague, M. L.; Lai, A. P.; Velasco, J.; Hughes, C. R.; Beyer, A. D.; Bockrath, M. W.; Lau, C. N.; Yeh, N. C. Evidence for Strain-Induced Local Conductance Modulations in Single-Layer Graphene on SiO_2. *Nano Lett.* **2009**, *9*, 2542–2546.
20. Xu, K.; Cao, P.; Heath, J. R. Scanning Tunneling Microscopy Characterization of the Electrical Properties of Wrinkles in Exfoliated Graphene Monolayers. *Nano Lett.* **2009**, *9*, 4446–4451.
21. Deng, D. H.; Pan, X. L.; Zhang, H.; Fu, Q.; Tan, D. L.; Bao, X. H. Freestanding Graphene by Thermal Splitting of Silicon Carbide Granules. *Adv. Mater.* **2010**, *22*, 2168–2171.
22. Pan, Y.; Zhang, H. G.; Shi, D. X.; Sun, J. T.; Du, S. X.; Liu, F.; Gao, H. J. Highly Ordered, Millimeter-Scale, Continuous, Single-Crystalline Graphene Monolayer Formed on Ru (0001). *Adv. Mater.* **2009**, *21*, 2777–2780.

23. Gao, L.; Guest, J. F.; Guisinger, N. P. Epitaxial Graphene on Cu(111). *Nano Lett.* **2010**, *10*, 3512–3516.
24. Rasool, H. I.; Song, E. B.; Allen, M. J.; Wassei, J. K.; Kaner, R. B.; Wang, K. L.; Weiller, B. H.; Gimzewski, J. K. Continuity of Graphene on Polycrystalline Copper. *Nano Lett.* **2011**, *11*, 251–256.
25. Wofford, J. M.; Nie, S.; McCarty, K. F.; Bartelt, N. C.; Dubon, O. D. Graphene Islands on Cu Foils: The Interplay between Shape, Orientation, and Defects. *Nano Lett.* **2010**, *10*, 4890–4896.
26. Zhang, Y. B.; Brar, V. W.; Wang, F.; Girit, C.; Yayon, Y.; Panlasigui, M.; Zettl, A.; Crommie, M. F. Giant Phonon-Induced Conductance in Scanning Tunneling Spectroscopy of Gate-Tunable Graphene. *Nat. Phys.* **2008**, *4*, 627–630.
27. Deshpande, A.; Bao, W.; Miao, F.; Lau, C. N.; LeRoy, B. J. Spatially Resolved Spectroscopy of Monolayer Graphene on SiO_2. *Phys. Rev. B* **2009**, *79*, (205411)1-6.
28. Chae, S. J.; Gunes, F.; Kim, K. K.; Kim, E. S.; Han, G. H.; Kim, S. M.; Shin, H. J.; Yoon, S. M.; Choi, J. Y.; Park, M. H.; *et al.* Synthesis of Large-Area Graphene Layers on Poly-Nickel Substrate by Chemical Vapor Deposition: Wrinkle Formation. *Adv. Mater.* **2009**, *21*, 2328–2333.
29. Spiecker, E.; Schmid, A. K.; Minor, A. M.; Dahmen, U.; Hollensteiner, S.; Jäger, W. Self-Assembled Formation of Nanofold Networks on Layered Crystal Surfaces during Metal Intercalation. *Phys. Rev. Lett.* **2006**, *96*, (086401)1-4.
30. Taylor, R. E.*et al. Thermal Expansion of Solids*; ASM International: Materials Park, OH, 1998; p 273.
31. Vázquez de Parga, A. L.; Calleja, F.; Borca, B.; Passeggi, J. M. C. G.; Hinarejos, J. J.; Guinea, F.; Miranda, R. Periodically Rippled Graphene: Growth and Spatially Resolved Electronic Structure. *Phys. Rev. Lett.* **2008**, *100*, (056807)1-4.
32. Guinea, F.; Katsnelson, M. I.; Vozmediano, M. A. H. Midgap States and Charge Inhomogeneities in Corrugated Graphene. *Phys. Rev. B* **2008**, *77*, (075422)1-8.
33. Elias, D. C.; Nair, R. R.; Mohiuddin, T. M. G.; Morozov, S. V.; Blake, P.; Halsall, M. P.; Ferrari, A. C.; Boukhvalov, D. W.; Katsnelson, M. I.; Geim, A. K.; *et al.* Control of Graphene's Properties by Reversible Hydrogenation: Evidence for Graphane. *Science* **2009**, *323*, 610–613.
34. de Parga, A. L. V.; Calleja, F.; Borca, B.; Passeggi, M. C. G.; Hinarejos, J. J.; Guinea, F.; Miranda, R. Periodically Rippled Graphene: Growth and Spatially Resolved Electronic Structure. *Phys. Rev. Lett.* **2008**, *100*, (056807)1-4.
35. Partoens, B.; Peeters, F. M. From Graphene to Graphite: Electronic Structure Around the *K* Point. *Phys. Rev. B* **2006**, *74*, (075404)1-11.
36. Yang, H.; Mayne, A. J.; Boucherit, M.; Comtet, G.; Dujardin, G.; Kuk, Y. Quantum Interference Channeling at Graphene Edges. *Nano Lett.* **2010**, *10*, 943–947.
37. Rutter, G. M.; Crain, J. N.; Guisinger, N. P.; Li, T.; First, P. N.; Stroscio, J. A. Scattering and Interference in Epitaxial Graphene. *Science* **2007**, *317*, 219–222.
38. Yan, K.; Peng, H. L.; Zhou, Y.; Li, H.; Liu, Z. F. Formation of Bilayer Bernal Graphene: Layer-by-Layer Epitaxy *via* Chemical Vapor Deposition. *Nano Lett.* **2011**, *11*, 1106–1110.